ACS APPLIED MATERIALS & INTERFACES

Research Article

www.acsami.org

A Comparative Study of Nano-SiO_2 and Nano-TiO_2 Fillers on Proton Conductivity and Dielectric Response of a Silicotungstic Acid–H_3PO_4–Poly(vinyl alcohol) Polymer Electrolyte

Han Gao and Keryn Lian*

Department of Materials Science and Engineering, University of Toronto, Toronto, Ontario, Canada M5S 3E4

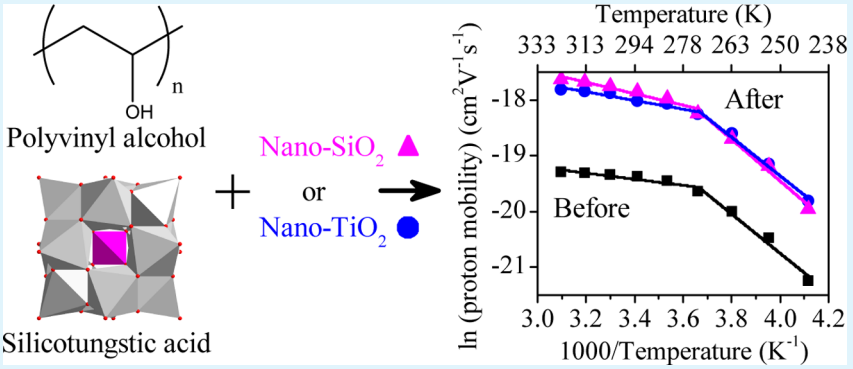

ABSTRACT: The effects of nano-SiO_2 and nano-TiO_2 fillers on a thin film silicotungstic acid (SiWA)–H_3PO_4–poly(vinyl alcohol) (PVA) proton conducting polymer electrolyte were studied and compared with respect to their proton conductivity, environmental stability, and dielectric properties, across a temperature range from 243 to 323 K. Three major effects of these fillers have been identified: (a) barrier effect; (b) intrinsic dielectric constant effect; and (c) water retention effect. Dielectric analyses were used to differentiate these effects on polymer electrolyte-enabled capacitors. Capacitor performance was correlated to electrolyte properties through dielectric constant and dielectric loss spectra. Using a single-ion approach, proton density and proton mobility of each polymer electrolyte were derived as a function of temperature. The results allow us to deconvolute the different contributions to proton conductivity in SiWA–H_3PO_4–PVA-based electrolytes, especially in terms of the effects of fillers on the dynamic equilibrium of free protons and protonated water in the electrolytes.

KEYWORDS: *silicotungstic acid, polyvinyl alcohol, polymer electrolyte, proton conductor, supercapacitor, nanofiller*

INTRODUCTION

Keggin-type heteropoly acids (HPAs), such as silicotungstic acid ($H_4SiW_{12}O_{40}$, SiWA), have demonstrated high solid-state proton conductivity at room temperature.[1−5] Two major factors contribute to proton conductivity: (i) Highly hydrogen-bonded conduction pathways in the crystal lattice facilitate fast proton transportation in SiWA. Such pathways result from a large number of cocrystallized water molecules in the crystal hydrate ($SiWA{\cdot}nH_2O$), leading to "quasi-liquid" states.[5−7] (ii) The dynamic dissociation of cocrystallized water molecules in the crystal hydrate via interactions with oxygen atoms of the Keggin anion increases the density of free protons as shown in the following reaction:[8,9]

$$(SiW_{12}O_{40})^{4-} + xH_2O \leftrightarrow [(SiW_{12}O_{40})(HO)]^{(4+x)-} + xH^+ \quad (a)$$

The protons, in the forms of H^+-nH_2O clusters (e.g., H_3O^+ or $H_5O_2^+$), are transferred by hopping from H^+-nH_2O donor sites to nH_2O acceptors in HPAs, demonstrating high proton conductivity (e.g., 0.027 S cm^{-1} for $SiWA{\cdot}28H_2O$).[2] HPA powders cannot easily form films and earlier studies relied on HPAs pressed into pellets, resulting in inhomogeneous particle contact.[3,4] More recently, HPAs have been immobilized in a thin film matrix to form proton-conducting composites for fuel cell or supercapacitor applications.[10−12]

A polymer-in-salt electrolyte comprising SiWA, H_3PO_4, and a poly(vinyl alcohol) matrix (referred as SiWA–H_3PO_4–PVA) has been demonstrated for ultrahigh rate supercapacitor applications.[13,14] The solid polymer electrolyte-based devices were able to charge and discharge up to 100 V s^{-1}, exceeding similar liquid-based devices[13] and exhibit a time constant of 10 ms.[14] Because of the high SiWA content and the low polymer content (ca. 10 wt.% PVA), the proton conduction mechanism in SiWA–H_3PO_4–PVA is dominated by the nature of the proton conductors rather than the segmental motion of its polymer chains. Accordingly, proton conduction in SiWA–H_3PO_4–PVA can be directly related to the amount of cocrystallized water molecules in SiWA. This also leads to a dependence of the performance of SiWA–H_3PO_4–PVA on

Received: October 14, 2013
Accepted: December 9, 2013
Published: December 9, 2013

relative humidity and on temperature.[13,15] Hygroscopic inorganic oxide fillers, such as SiO_2 and TiO_2, can act as water retention agents in polymer electrolytes through strengthening of hydrogen bond interactions between water molecules and hydroxyl groups on the filler surface.[15−17] The effects of such fillers on the environmental stability of proton-conducting polymer electrolytes have been characterized in many studies.[18−22] Nevertheless, the functions and impacts of these nonconductive fillers on proton conduction, especially in HPA-based polymer electrolyte systems, are yet to be understood.

Dielectric relaxation analysis is a useful tool for obtaining the characteristics of ionic and molecular motions and interactions. The frequency-dependent response of an electrolyte is measured in complex impedance (Z^*) and permittivity (ε^*), which reflect the motion of mobile ions and dipoles. A schematic diagram of the variation of dielectric constant (ε_r') and dielectric loss (ε_r'') as a function of frequency for a polymer-in-salt electrolyte is shown in Figure 1. Due to the low

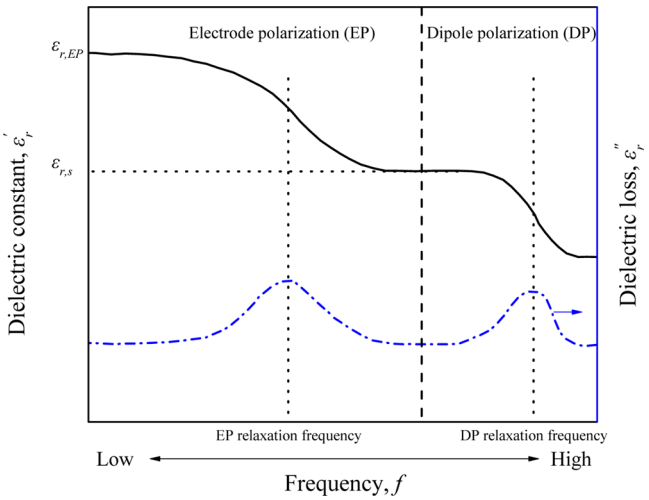

Figure 1. Schematic diagram of dielectric constant (ε_r') and dielectric loss response (ε_r'') for a polymer-in-salt electrolyte exhibiting dipole polarization and electrode polarization as a function of frequency.

polymer content and limited chain movements in a polymer-in-salt electrolyte, polarization caused by polymer main chain and/or side chain motions is small and negligible. Under such conditions, the two dominating types of polarization are dipole polarization at high frequencies and electrode polarization at low frequencies.

Dipole polarization derives mainly from the molecules of the ionic conductor and/or additives with permanent dipole moments, while electrode polarization is caused by the accumulation of ions at the blocking electrode surface (i.e., formation of the electrical double layer). In Figure 1, the corresponding dielectric constant at high frequencies (i.e., without electrode polarization) is denoted as static dielectric constant ($\varepsilon_{r,s}$) and the dielectric constant at low frequencies (i.e., with electrode polarization) is denoted as low frequency dielectric constant ($\varepsilon_{r,EP}$). In supercapacitors, a high $\varepsilon_{r,s}$ reflects a high intrinsic capacitance similar to the capacitance of an electrolytic capacitor, whereas a high $\varepsilon_{r,EP}$ reflects a greater amount of stored charge at the electrode/electrolyte interface (i.e., an electrical double-layer capacitor). The capacitance from electrode polarization ($\varepsilon_{r,EP}$) is generally much greater than the intrinsic capacitance and is the interest of supercapacitors. In the dielectric loss vs frequency curve, two dielectric loss peaks can be observed. These peaks correspond to (a) the relaxation of dipole polarization and (b) the relaxation of electrode polarization. Both loss peaks result from energy dissipation when the polarization lags behind the applied electric field. In addition, the position of the ε_r'' peak represents the relaxation frequency. A loss peak with small magnitude and high relaxation frequency (i.e., small loss and fast response) is desirable for a capacitor. In general, a capacitor can be viewed as a macroscopic dipole with charge separation as a result of electrode polarization at low frequencies, and can be represented by a simple Debye relaxation in the Macdonald and Coelho model.[23−26]

Dipole relaxation and dielectric response have been studied for different HPAs and their salts,[5,27] and have been shown to fit well in the Debye relaxation model. Dielectric response and relaxation of polymers such as PVA, poly(ethylene oxide), poly(vinylidene fluoride), poly(imidazolium acrylate), polystyrene, and their complexes have also been well characterized.[23,28−35] However, the effects of inorganic oxide fillers, such as TiO_2 and SiO_2, in polymer-in-salt electrolytes and their effects on the macroscopic charge transportation have not been quantified. In addition, the difference in the intrinsic dielectric constant of TiO_2 (80) and SiO_2 (3.9)[36] could also affect the static dielectric constant ($\varepsilon_{r,s}$) of the electrolyte film, impacting the intrinsic capacitance of a polymer electrolyte-enabled cell at high frequencies. This is also of interest because of the possibility to enhance supercapacitor performance at ultrahigh rates.

In this study, the effects of nano-TiO_2 and nano-SiO_2 fillers on a SiWA−H_3PO_4−PVA polymer-in-salt electrolyte were characterized and compared in terms of their proton conductivity, environmental stability, and dielectric properties. Our goal was to derive the macroscopic charge transportation properties in the SiWA-based polymer electrolytes by leveraging dielectric analyses using the Macdonald and Coelho model. In particular, the impact of TiO_2 and SiO_2 fillers on free proton density and their mobility in the polymer electrolytes were investigated and quantified.

EXPERIMENTAL SECTION

Materials and Preparation. SiWA−H_3PO_4−PVA/TiO_2 and SiWA−H_3PO_4−PVA/SiO_2 polymer electrolytes were fabricated from a precursor solution prepared by mixing a polyvinyl alcohol (PVA, Aldrich MW = 145 000) solution with $H_4SiW_{12}O_{40}$ (SiWA, Alfa Aesar) and orthophosphoric acid (H_3PO_4, Alfa Aesar). TiO_2 (15 nm powder, Alfa Aesar) or SiO_2 (10−20 nm powder, Alfa Aesar) was added to the solution as inorganic oxide filler. The processed SiWA−H_3PO_4−PVA/TiO_2 and SiWA−H_3PO_4−PVA/SiO_2 films had a composition of 80 wt % SiWA, 10 wt % H_3PO_4, 5 wt % PVA, and 5 wt % TiO_2 or SiO_2, assuming most of the water was removed in the process. For comparison, we also studied a SiWA−H_3PO_4−PVA film with the same percentage of ionic conductive materials and 10 wt.% PVA. The thickness of the electrolyte films was controlled to be ca. 90 μm.

Cell Fabrication. To determine the performance of our polymer electrolytes, stainless steel foil (50 μm thick, Type 304, McMaster-Carr) was used as smooth metallic electrode. The geometric area of all electrodes was 1 cm^2. Cells in two-electrode configuration (stainless steel/polymer electrolyte/stainless steel) were assembled in the following steps:[15] (i) The electrodes were coated with the electrolyte precursor solution via solution casting and air-dried to form a thin film. (ii) Capacitor cells were fabricated by fusing two electrolyte-coated electrodes together for 20 min under 20 to 30 kPa pressure at ambient temperature to ensure good interfacial contact.

dx.doi.org/10.1021/am4045103 | ACS Appl. Mater. Interfaces 2014, 6, 464−472

In addition, a liquid H_2SO_4 cell was constructed by sandwiching a presoaked separator paper (150 μm thick, 30 wt % liquid H_2SO_4) between two stainless steel electrodes as a baseline for cyclic voltammetry (CV) characterization.

Dielectric Characterizations of Polymer Electrolytes. Cells using polymer electrolytes were characterized using CV and ac impedance on a CHI 760C bipotentiostat. An Espec SH-241 temperature/humidity chamber was used for tests at various temperatures and humidity levels. The key parameters of interest are: proton conductivity (σ), dielectric constant (ε_r'), dielectric loss (ε_r''), dielectric time constant (τ), free proton density (p_0), and mobility (μ).

The equivalent series resistance (ESR) of the capacitors was extracted from the ac impedance measurements. Proton conductivity is the dc conductivity of the polymer electrolyte and was obtained based on the geometric surface area (A) and the thickness of the polymer electrolyte (d) using eq 1.

$$\sigma = q\mu p_0 = \frac{d}{\mathrm{ESR} \times A} \tag{1}$$

where q is elementary charge, μ is proton mobility, and p_0 is proton density. The reported conductivity for each electrolyte was based on the average measurements of at least five cells.

Areal capacitance of the solid cells was calculated using charge divided by voltage window and geometric surface area. Dielectric properties of each electrolyte were also obtained from ac impedance measurements in the frequency range from 100 kHz to 1 Hz. The solid sandwich cell can be considered as a capacitor such that the real part of the capacitance can be extracted using its impedance data.[37] The dielectric constant ε_r' is extracted using eq 2

$$\varepsilon_r' = \frac{C'}{C_0} = \frac{-Z''}{2\pi f|Z|^2}\frac{d}{\varepsilon_0 A} \tag{2}$$

where C' is the real part of the cell capacitance, C_0 is the vacuum capacitance, Z is the complex impedance, Z'' is the imaginary part of the complex impedance, and ε_0 is the relative permittivity of vacuum. The dielectric loss (ε_r'') can be determined from eq 3

$$\varepsilon_r'' = (\varepsilon_r')\left(-\frac{1}{\tan\theta}\right) \tag{3}$$

where θ is the phase angle (or phase shift) of a capacitor.

The change in the electric field will cause dielectric relaxation of the polymer electrolytes. The lag between the change of the applied electric field and the dielectric polarization of the polymer electrolyte can be represented by a characteristic dielectric time constant (τ). In general, τ is directly related to the dielectric constant and dc conductivity through eq 4:

$$\tau = \frac{\varepsilon_r'\varepsilon_0}{\sigma} \tag{4}$$

At high frequencies, the dielectric constant of a material is dominated by its dipole polarization. Thus, the static dielectric time constant (τ_s) of a material is related to the static dielectric constant. Conversely, electrode polarization occurs at the blocking electrodes at low frequencies, and its dielectric time constant (τ_{EP}) is related to the low frequency dielectric constant, as shown in eq 4a.

$$\tau_s = \frac{\varepsilon_{r,s}\varepsilon_0}{\sigma} \qquad \tau_{EP} = \frac{\varepsilon_{r,EP}\varepsilon_0}{\sigma} \tag{4a}$$

Since a solid capacitor cell can also be viewed as a macroscopic dipole, Debye relaxation is used to represent the dielectric relaxation response of the polymer electrolytes as shown in eq 5

$$\varepsilon_{r,EP}^* = \varepsilon_{r,s} + \frac{\varepsilon_{r,EP} - \varepsilon_{r,s}}{1 + 2\pi f\tau_{EP}j} \tag{5}$$

where $\varepsilon_{r,EP}^*$ is the complex form of the dielectric constant with electrode polarization.

Free Ion Density and Mobility. The free proton density and their mobility were evaluated from ac impedance measurements under presence of electrode polarization. The free ions in all three polymer electrolytes were assumed to be protons due to the high SiWA content and the large and relatively immobile Keggin anions.[5] The proton transference number in SiWA is close to unity, which is also true for the polymer electrolytes. A single ion approach[23] was used, where the scale of the double layer is controlled by the Debye length (L_D)

$$L_D = \frac{1}{q}\left(\frac{\varepsilon_{r,s}\varepsilon_0 kT}{p_0}\right)^{1/2} \tag{6}$$

where k is Boltzmann's constant.

In the Macdonald and Coelho model,[24−26] the ratio of electrolyte thickness (d) and $2L_D$ is defined as M as shown in eq 7.

$$M = \frac{d}{2L_D} = \frac{qd}{2}\left(\frac{p_0}{\varepsilon_{r,s}\varepsilon_0 kT}\right)^{1/2} = \frac{\varepsilon_{r,EP}}{\varepsilon_{r,s}} = \frac{\tau_{EP}}{\tau_s} \tag{7}$$

Rearranging eq 7 and combining with eq 4, one can obtain τ_{EP} in eq 8.

$$\tau_{EP} = M\tau_s = \frac{qd}{2}\left(\frac{p_0}{\varepsilon_{r,s}\varepsilon_0 kT}\right)^{1/2}\frac{\varepsilon_{r,s}\varepsilon_0}{p_0 q\mu} = \frac{d}{2\mu}\left(\frac{\varepsilon_{r,s}\varepsilon_0}{p_0 kT}\right)^{1/2} \tag{8}$$

The free proton density, p_0, can then be obtained by rearranging eq 8.

$$p_0 = \frac{4\tau_{EP}^2 kT\sigma}{q^2 d^2 \tau_s} \tag{9}$$

Mobility can be determined from dc conductivity and free proton density using eq 1.

While eqs 6−9 represent proton density (or proton mobility) at a given temperature, the Arrhenius relation (eq 10) can be used to describe proton density and proton conductivity (and thus proton mobility) at different temperatures:

$$A_0 = A_\infty \exp\left(\frac{-E_a}{RT}\right) \tag{10}$$

where A_0 can be proton conductivity, proton density, or proton mobility, A_∞ is a pre-exponential factor, R is the gas constant, and E_a is activation energy. Free proton density and mobility of the polymer electrolytes at low temperatures of 243 and 253 K were directly calculated using eqs 9 and 1. At higher temperatures, the proton density was obtained by linear fitting using eq 10, and mobility was calculated based on dc conductivity and free proton density using eq 1.

RESULTS AND DISCUSSION

The effects of TiO_2 and SiO_2 on SiWA−H_3PO_4−PVA polymer electrolytes were first investigated under ambient conditions and then in controlled temperature environments. At room temperature, the proton conductivity of each electrolyte was monitored over time to determine environmental stability. The CVs of all solid cells were compared to differentiate any observed reduction in capacitance. In controlled temperature environments, the capacitance of solid cells was evaluated under a high scan rate to investigate the effect of the intrinsic dielectric constant of the fillers. Dielectric properties were used to extract the free proton density and the mobility of the electrolytes from dc conductivity at different temperatures. Table 1 lists the relationship between solid capacitor performance and the polymer electrolyte properties of interest. Since all solid cells share the same electrodes, cell geometry, and configuration, comparisons of cell performance can be directly related to the electrolyte material properties.

Proton Conductivity at Room Temperature. Proton conductivity of the polymer electrolytes with and without fillers

dx.doi.org/10.1021/am4045103 | ACS Appl. Mater. Interfaces 2014, 6, 464−472

Table 1. Solid Capacitor Performance Parameters and Related Polymer Electrolyte Material Properties

capacitor performance	related electrolyte material properties
high frequency cell capacitance	static dielectric constant ($\varepsilon_{r,s}$)
low frequency cell capacitance	low frequency dielectric constant ($\varepsilon_{r,EP}$)[a]
equivalent series resistance (ESR)	proton conductivity (σ)
RC time constant	relaxation time of electrode polarization

[a]Low frequency cell capacitance corresponds to the extent of electrode polarization (i.e., $\varepsilon_{r,EP} - \varepsilon_{r,s}$). However, since $\varepsilon_{r,EP}$ is typically orders of magnitude larger than $\varepsilon_{r,s}$, the latter term can be neglected.

was monitored over a period of 2 months under ambient conditions as shown in Figure 2. The average conductivity of

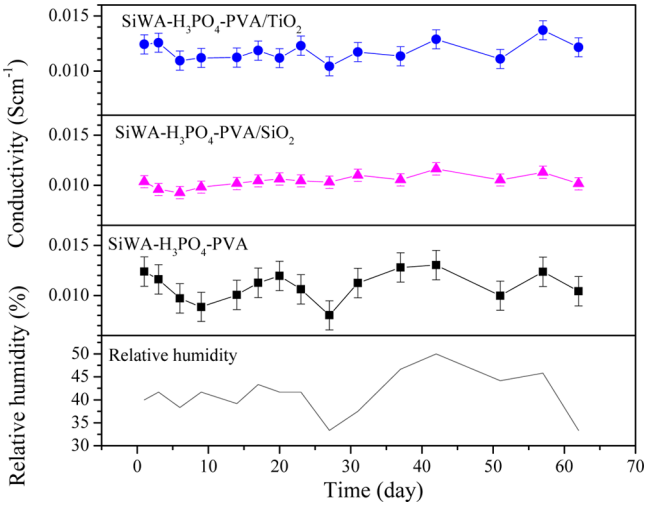

Figure 2. Proton conductivity tracking of polymer electrolytes SiWA–H_3PO_4–PVA/TiO_2 (blue circle), SiWA–H_3PO_4–PVA/SiO_2 (magenta triangle), and SiWA–H_3PO_4–PVA (black square) over time under ambient conditions.

SiWA–H_3PO_4–PVA was 0.011 S cm^{-1}. SiWA–H_3PO_4–PVA/TiO_2 and SiWA–H_3PO_4–PVA/SiO_2 had similar average conductivity (0.011 and 0.010 S cm^{-1}, respectively). However, the filler-free electrolyte showed a strong fluctuation in conductivity with relative humidity compared to the electrolytes with fillers. Although the SiO_2-containing electrolyte has the lowest conductivity among the three electrolytes, it demonstrated the best stability with the least fluctuation. This can be explained by a higher concentration of surface hydroxyl groups available on SiO_2 leading to a stronger water retention effect than that of TiO_2. Nevertheless, the addition of TiO_2 improved stability over SiWA–H_3PO_4–PVA.

Cell Capacitance at Room Temperature. To determine the effects of TiO_2 and SiO_2 fillers on cell capacitance, CVs of three solid cells with SiWA–H_3PO_4–PVA, SiWA–H_3PO_4–PVA/SiO_2, and SiWA–H_3PO_4–PVA/TiO_2 electrolytes were overlaid in Figure 3 together with the CV of a liquid H_2SO_4 cell. All four cells demonstrated a highly capacitive response with near rectangular shape in an ambient environment. The liquid H_2SO_4 cell demonstrated the highest capacitance of 29 μFcm^{-2} at 1 V s^{-1}. Among the three polymer electrolyte-based cells, the SiWA–H_3PO_4–PVA cell had the highest cell capacitance (27 μFcm^{-2}), comparable to the liquid H_2SO_4 cell. The TiO_2- and SiO_2-containing cells showed lower capacitance, 25 and 21 μFcm^{-2}, respectively.

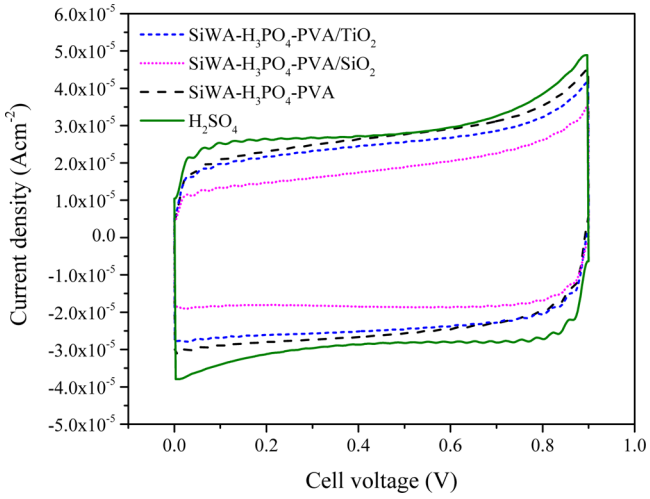

Figure 3. CV comparison of SiWA–H_3PO_4–PVA/TiO_2-based (short dash), SiWA–H_3PO_4–PVA/SiO_2-based (dot), SiWA–H_3PO_4–PVA-based (long dash), and liquid H_2SO_4 (line) metallic cells at 25 °C and 50% relative humidity (scan rate 1 V s^{-1}).

The capacitance of each solid cell was measured and compared as a function of frequency in Figure 4. All cells

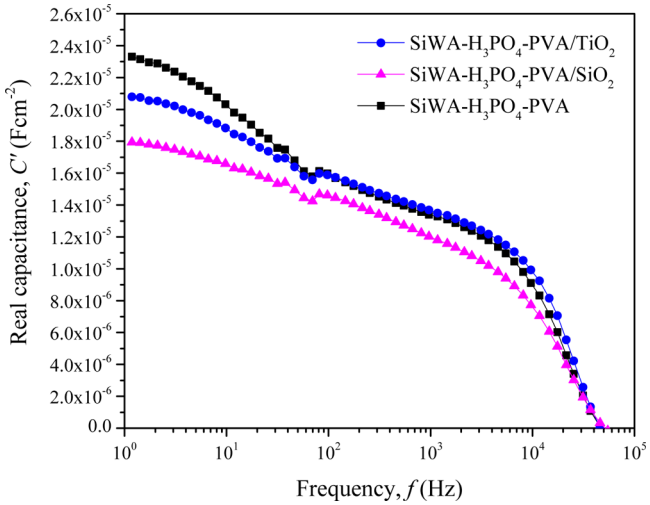

Figure 4. Real part of ac capacitance (C') of SiWA–H_3PO_4–PVA/TiO_2-based (blue circle), SiWA–H_3PO_4–PVA/SiO_2-based (magenta triangle), and SiWA–H_3PO_4–PVA-based (black square) metallic cells at 25 °C and 50% relative humidity.

showed increased capacitance toward low frequencies. At low frequencies, both TiO_2- and SiO_2-containing cells showed lower capacitance than that of the SiWA–H_3PO_4–PVA-based cell, similar to the CV results in Figure 3. This may be due to the physical blocking of the electrode surface by the presence of nonconductive fillers (referred to as barrier effect). SiO_2 showed a stronger barrier effect when compared to TiO_2, resulting in a greater reduction in cell capacitance at a low scan rate of 1 V s^{-1}.

Temperature Dependence of Cell Capacitance. To investigate the influence of TiO_2 and SiO_2 fillers on cell performance at different temperatures, the cells were tested at an ultrahigh rate of 5000 V s^{-1} from 243 to 323 K, as depicted in Figure 5a–c. At higher temperatures (i.e., T > 273 K), all cells showed rectangular CV profiles, exhibiting rapid charge/

dx.doi.org/10.1021/am4045103 | ACS Appl. Mater. Interfaces 2014, 6, 464–472

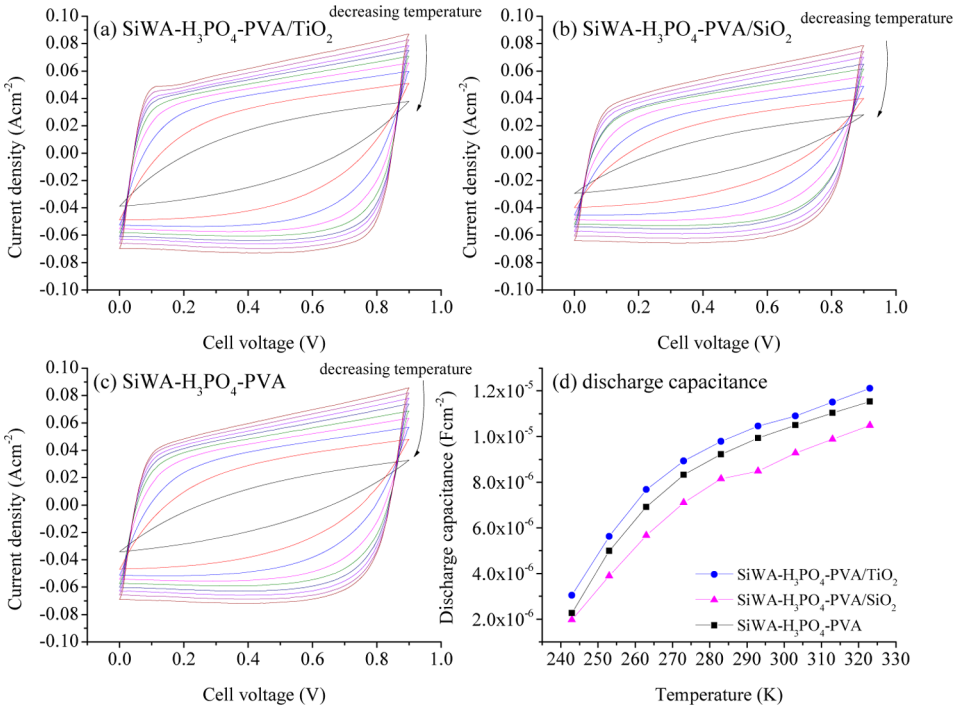

Figure 5. CV overlays of (a) SiWA−H_3PO_4−PVA/TiO_2-based, (b) SiWA−H_3PO_4−PVA/SiO_2-based, (c) SiWA−H_3PO_4−PVA-based metallic cells at 323 K (outermost) to 243 K (innermost), and (d) discharge capacitance of SiWA−H_3PO_4−PVA/TiO_2-based (blue circle), SiWA−H_3PO_4−PVA/SiO_2-based (magenta triangle), and SiWA−H_3PO_4−PVA-based (black square) metallic cells at 5000 V s^{-1} scan rate.

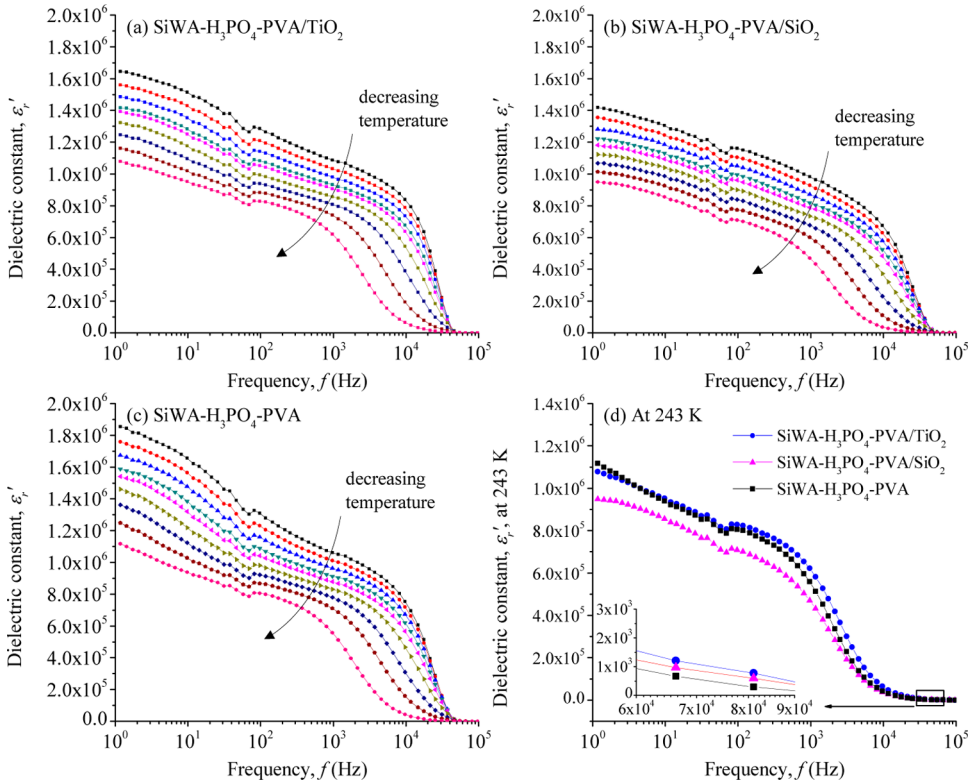

Figure 6. Dielectric constant of polymer electrolytes (a) SiWA−H_3PO_4−PVA/TiO_2, (b) SiWA−H_3PO_4−PVA/SiO_2, (c) SiWA−H_3PO_4−PVA, from 323 to 243 K, and (d) a comparison of the dielectric constant of SiWA−H_3PO_4−PVA/TiO_2 (blue circle), SiWA−H_3PO_4−PVA/SiO_2 (magenta triangle), and SiWA−H_3PO_4−PVA (black square) at 243 K.

discharge characteristics. A reduction in cell capacitance with decreasing temperature was observed in all cells. Tilted voltammograms were observed at low temperatures, resultant from a significant increase in cell ESR. Nevertheless, the SiWA−H_3PO_4−PVA/TiO_2-based cell exhibited less distortion relative to the other two cells at lower temperatures. For a

dx.doi.org/10.1021/am4045103 | ACS Appl. Mater. Interfaces 2014, 6, 464−472

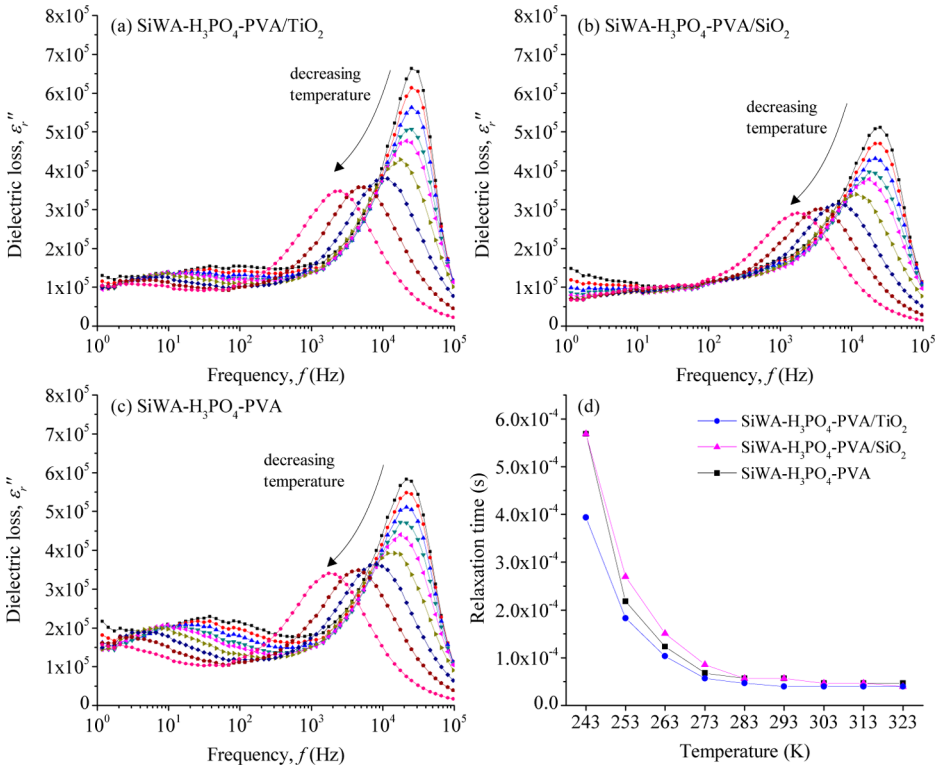

Figure 7. Dielectric loss of polymer electrolytes (a) SiWA–H_3PO_4–PVA/TiO_2, (b) SiWA–H_3PO_4–PVA/SiO_2, (c) SiWA–H_3PO_4–PVA, from 323 to 243 K, and (d) relaxation time of electrode polarization for SiWA–H_3PO_4–PVA/TiO_2, SiWA–H_3PO_4–PVA/SiO_2, and SiWA–H_3PO_4–PVA at different temperatures.

better comparison of the three polymer electrolytes, the discharge capacitance of each cell at different temperatures was extracted and is shown in Figure 5d. The SiO_2-containing cell had the lowest capacitance, similar to what was observed at a 1 V s^{-1} scan rate (see Figure 3). Although the SiWA–H_3PO_4–PVA-based cell showed a higher capacitance than that of the cell with TiO_2 at 1 V s^{-1}, this situation was reversed at 5000 V s^{-1}. At a high scan rate, SiWA–H_3PO_4–PVA/TiO_2 had consistently higher cell capacitance compared to both SiWA–H_3PO_4–PVA and SiWA–H_3PO_4–PVA/SiO_2, across the entire temperature range.

Dielectric Analyses. Dielectric analyses were performed based on ac impedance measurements to derive the macroscopic charge transportation properties in the polymer electrolytes with and without fillers and to identify the origin of the variations in capacitance of the solid cells between Figures 3 and 5. The dielectric constant of each polymer electrolyte is plotted from 243 to 323 K based on eq 2 and is shown in Figure 6a–c. The dielectric loss spectra (from eq 3) are plotted against frequency for these electrolytes in Figure 7a–c.

All three polymer electrolytes showed high apparent dielectric constants at low frequencies (Figure 6a–c) related to the electrode polarization. As frequency increases, the dielectric constant generally decreases, similar to the trend in the real part of capacitance (C') vs frequency (Figure 4). All three solid cells showed resonance behavior at the high frequency end from the influence of residual inductance. Moreover, the dielectric constants decreased with the decrease of temperature throughout the frequency range. At any given temperature, the low frequency dielectric constants of SiWA–H_3PO_4–PVA were higher than those of SiWA–H_3PO_4–PVA with fillers, in agreement with the dc capacitance measured at 1 V s^{-1} (Figure 3).

To minimize the influence of self-resonance on the dielectric response of the polymer electrolytes, the dielectric constants at a low temperature were first analyzed, so that the effects of fillers could be more clearly isolated. Plots of the dielectric constants of SiWA–H_3PO_4–PVA, SiWA–H_3PO_4–PVA/TiO_2, and SiWA–H_3PO_4–PVA/SiO_2 vs frequency at 243 K were overlaid in Figure 6d. At this low temperature, both $\varepsilon_{r,EP}$ and $\varepsilon_{r,s}$ could be obtained from Figure 6d, where $\varepsilon_{r,EP}$ was the dielectric constant at 1 Hz and $\varepsilon_{r,s}$ was extrapolated from the steady-state dielectric constant between 70 kHz and 90 kHz. At the low frequency region, $\varepsilon_{r,EP}$ decreased in the order of SiWA–H_3PO_4–PVA > SiWA–H_3PO_4–PVA/TiO_2 > SiWA–H_3PO_4–PVA/SiO_2, showing the same trend as observed in Figures 3 and 4. At high frequencies, the dielectric constants of the three polymer electrolytes showed a different trend, with SiWA–H_3PO_4–PVA/TiO_2 the highest, followed by SiWA–H_3PO_4–PVA/SiO_2 and SiWA–H_3PO_4–PVA, as expected from the intrinsic dielectric constant of TiO_2 (80) and SiO_2 (3.9).[36] At high frequencies, the dielectric constant is dominated by the molecular dipole polarization of inorganic solids such as SiWA or filler. The incorporation of fillers with high molecular polarizability increased the static dielectric constant of the polymer electrolytes. This also explained the observation in Figure 5d that a SiWA–H_3PO_4–PVA/TiO_2-based cell could store and deliver more charge at a high voltage scan rate. Even at high frequencies, the dielectric constants were still in the order of 10^2–10^3. This was due to the heterogeneous nature of the polymer composite, where interfacial polarization[38] among SiWA, PVA, fillers, and even water molecules all contributed to the dielectric constants of the electrolytes.

dx.doi.org/10.1021/am4045103 | ACS Appl. Mater. Interfaces 2014, 6, 464–472

Since the dielectric loss at high frequencies results from the energy dissipation from the lag between the charge separation in the polymer electrolytes and the ac electric field, a shorter relaxation time suggests a faster response of the cell. This characteristic relaxation time can be used to evaluate rate performance of a cell, in close analogy to the RC time constant of a supercapacitor. For example, among capacitors with similar capacitance, the one with the lowest ESR will have a faster transition from a resistive-dominated state to a capacitive-dominated state, demonstrating the smallest RC time constant.[37] Figure 7d shows the relaxation time of electrode polarization for all three polymer electrolytes with respect to temperature, which all increased with a decrease in temperature. At high temperatures, there was little difference among the three polymer electrolytes in their response times. At low temperatures (i.e., $T < 273$ K), the TiO_2-containing electrolyte exhibited a faster response over both SiWA–H_3PO_4–PVA and SiWA–H_3PO_4–PVA/SiO_2, implying a better rate capability of the SiWA–H_3PO_4–PVA/TiO_2-based devices. From Figures 5d and 6d, it is clear that SiWA–H_3PO_4–PVA/TiO_2 demonstrated the fastest response and had the highest dielectric constants and capacitance at low temperatures. Therefore, based on the RC model, SiWA–H_3PO_4–PVA/TiO_2 should possess the highest proton conductivity at low temperatures.

Temperature Dependence of Proton Conductivity. The relaxation frequencies of electrode polarization in Figure 7 are closely related to the cell ESR and, thus, the proton conductivity of the electrolytes at the respective temperature. Proton conductivity (σ) at different temperatures for all three electrolytes was further studied via Arrhenius plots in Figure 8.

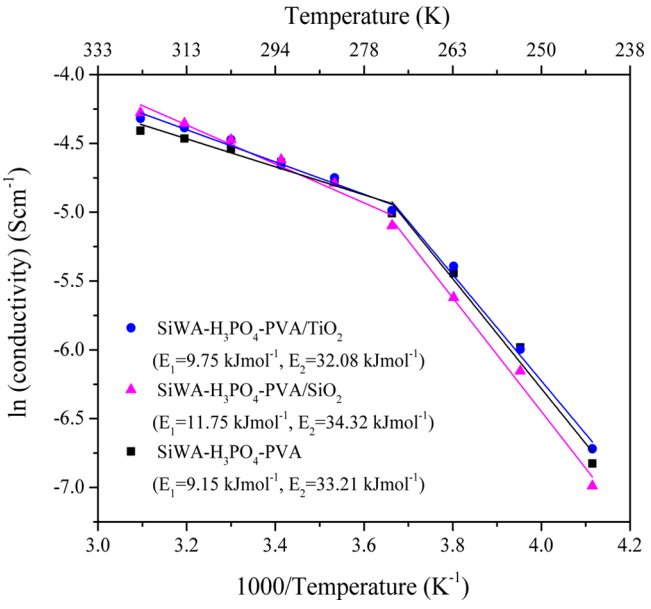

Figure 8. Temperature dependence of polymer electrolyte conductivity for SiWA–H_3PO_4–PVA/TiO_2 (blue circle), SiWA–H_3PO_4–PVA/SiO_2 (magenta triangle), and SiWA–H_3PO_4–PVA (black square) at 50% relative humidity.

The proton conductivity plots in Figure 8 can be divided into two regions, above and below 273 K. The high linearity in both regions confirmed the conduction of protons via Grotthuss (or hopping) mechanism. At temperatures above 273 K, the activation energy of SiWA–H_3PO_4–PVA was 9.15 kJmol^{-1}. The addition of TiO_2 or SiO_2 slightly increased the activation energy within this temperature range due to the barrier effect.

At temperatures below 273 K, an increase in activation energy for all three polymer electrolytes was observed (Figure 8). The activation energy increased to 33.21, 34.32, and 32.08 kJ mol^{-1} for SiWA–H_3PO_4–PVA, SiWA–H_3PO_4–PVA/SiO_2, and SiWA–H_3PO_4–PVA/TiO_2, respectively. Since fast proton transportation is enabled by the rotation of water molecules within the SiWA structure, the motion of water molecules might be limited at temperatures below the freezing point. This would render a higher energy barrier against structural reorganization/reorientation of water molecules and H^+-$n$$H_2O$ clusters. Under such conditions, an enhancement in proton conductivity is mainly due to the increase in proton density rather than proton mobility. Utilizing the Arrhenius plot in Figure 8 and eq 9 at the respective temperatures, we could further extract proton density (p_0) and proton mobility (μ) from each electrolyte to study the influence and the contributions of SiO_2 and TiO_2 fillers.

Free Proton Density and Mobility. The proton density of each electrolyte was first calculated from the respective dielectric time constants (τ_s and τ_{EP}) using eq 4. We started with low temperatures of 243 and 253 K to obtain τ_s more accurately, with minimum influence of self-resonance at high frequencies. The calculated p_0 and μ at 243 and 253 K are listed in Table 2. Proton density was lower for SiWA–H_3PO_4–PVA with fillers than for the electrolytes without fillers. This may be caused by a reduction of water molecule dissociation in the presence of fillers. In general, the equilibrium between protonated water and free protons in HPAs was assumed as[5]

$$H_5O_2^+ \leftrightarrow H_3O^+ + H_2O \leftrightarrow H^+ + 2H_2O\uparrow \qquad \text{(b)}$$

Dehydration in SiWA will shift the equilibrium toward the right to generate more free protons. However, this dehydration process may reduce the pathway for protons and thus limit proton transportation and decrease proton mobility.

With the addition of TiO_2 or SiO_2, reaction b becomes more difficult to proceed to the right, so that there are fewer free protons in SiWA–H_3PO_4–PVA/TiO_2 and SiWA–H_3PO_4–PVA/SiO_2 than in their filler-free counterparts. As a consequence of the lower water retention effect, the filler-free SiWA–H_3PO_4–PVA had the largest p_0 among the three electrolytes. Also shown in Table 2 is the mobility for the three polymer electrolytes. The dissociation of $H_5O_2^+$ ions, in spite of generating more free protons, might have reduced the proton transport pathway. Among the three polymer electrolytes, SiWA–H_3PO_4–PVA showed the lowest ion mobility, whereas both SiWA–H_3PO_4–PVA/TiO_2 and SiWA–H_3PO_4–PVA/SiO_2 demonstrated higher proton mobility. This trend was also observed for proton density and mobility of the three electrolytes at 253 K (Table 2).

Since $\varepsilon_{r,s}$ is difficult to extract from Figure 6a–c at temperatures above 253 K due to the lack of a clear plateau at the high frequency region, an indirect approach was chosen for calculating proton density. We first leveraged the proton density at 243 and 253 K (Table 2) and the Arrhenius relationship (Figure 8) to obtain the proton density at temperatures from 263 to 323 K, and then calculated proton mobility using dc conductivity at respective temperatures using eq 1. Figure 9 shows the mobility of all three polymer electrolytes as a function of temperature. Both SiWA–H_3PO_4–PVA/SiO_2 and SiWA–H_3PO_4–PVA/TiO_2 possess higher proton mobility than SiWA–H_3PO_4–PVA over the entire

dx.doi.org/10.1021/am4045103 | ACS Appl. Mater. Interfaces 2014, 6, 464–472

Table 2. Free Protons (p_0), Mobility (μ), and Conductivity (σ) of SiWA−H_3PO_4−PVA, SiWA−H_3PO_4−PVA/TiO_2, and SiWA−H_3PO_4−PVA/SiO_2 at 243 and 253 K

T (K)	polymer electrolyte	p_0 (cm^{-3})	μ ($cm^2\ V^{-1}\ s^{-1}$)	σ ($S\ cm^{-1}$)
243	SiWA−H_3PO_4−PVA	1.14×10^{25}	5.96×10^{-10}	1.09×10^{-3}
	SiWA−H_3PO_4−PVA/TiO_2	3.02×10^{24}	2.49×10^{-9}	1.21×10^{-3}
	SiWA−H_3PO_4−PVA/SiO_2	2.66×10^{24}	2.17×10^{-9}	9.22×10^{-4}
253	SiWA−H_3PO_4−PVA	1.22×10^{25}	1.28×10^{-9}	2.50×10^{-3}
	SiWA−H_3PO_4−PVA/TiO_2	3.22×10^{24}	4.82×10^{-9}	2.51×10^{-3}
	SiWA−H_3PO_4−PVA/SiO_2	2.83×10^{24}	4.68×10^{-9}	2.12×10^{-3}

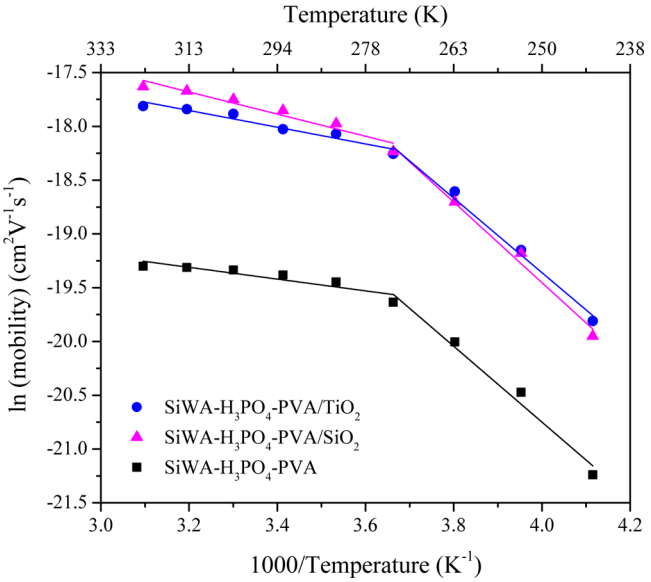

Figure 9. Temperature dependence of free proton mobility in polymer electrolytes SiWA−H_3PO_4−PVA (black square), SiWA−H_3PO_4−PVA/TiO_2 (blue circle), and SiWA−H_3PO_4−PVA/SiO_2 (magenta triangle) from 243 to 323 K.

temperature range. Although the effect of water retention below 273 K is much less significant than at higher temperatures, both SiO_2- and TiO_2-containing electrolytes still showed much higher proton mobility than their filler-free counterpart. This suggests the addition of SiO_2 and TiO_2 could facilitate proton transportation not only by the retention of water molecules but also through their hydroxyl-rich nanoparticle surfaces in filler-containing electrolytes.

While the proton mobility of the SiO_2 and TiO_2-containing electrolytes is identical below 273 K, above freezing temperature the proton mobility of SiWA−H_3PO_4−PVA/SiO_2 exceeded that of SiWA−H_3PO_4−PVA/TiO_2. At 323 K, the proton mobility of the SiO_2-containing electrolyte was more than 20% higher than the mobility of the TiO_2-containing electrolyte. This might be the result of stronger water retention in the form of H_3O^+ or $H_5O_2^+$ in the presence of SiO_2, leading to a more stable proton transport network in the nano-SiO_2-containing electrolyte at higher temperatures.

While proton density and mobility are both important contributors to proton conduction, they do not exhibit a clear relationship in the HPA-based polymer electrolyte systems, especially in the presence of fillers. The dissociation of $H_5O_2^+$ ions will increase the proton density, but lower the proton mobility and conductivity. For example, the proton conductivity of $H_3PW_{12}O_{40}{\cdot}21H_2O$ (another common HPA) was found to be 2 orders of magnitude higher than that of $H_3PW_{12}O_{40}{\cdot}6H_2O$.[1,5] This was attributed to higher proton mobility in the higher hydrates despite that more free protons were available in the hexahydrate. An opposite example shows that the proton conductivity of anhydrous $H_3PW_{12}O_{40}$ was 5 orders of magnitude higher than for its hexahydrate form, caused by a release of a large number of protons after calcination.[27] Therefore, a high performance proton conducting electrolyte for supercapacitors will require a balance between $H_5O_2^+$ and H^+ for optimum proton density and mobility without sacrificing cell capacitance. The addition of SiO_2 or TiO_2 promotes such optimization with respect to water retention and intrinsic capacitance, as demonstrated in this work.

CONCLUSIONS

In this report, the effects of SiO_2 and TiO_2 fillers on SiWA−H_3PO_4−PVA polymer electrolytes were characterized. Three major effects have been identified: (a) The barrier effect of the filler is a direct result of the reduction in extent of electrode polarization, leading to lower double layer capacitance in a supercapacitor. Among the two fillers, SiO_2 showed a stronger barrier effect than TiO_2. (b) The intrinsic dielectric constant effect is related to the static dielectric constants of polymer electrolytes. The higher intrinsic dielectric constant of TiO_2 resulted in a higher capacitance of SiWA−H_3PO_4−PVA/TiO_2-based cells over that of SiWA−H_3PO_4−PVA/SiO_2- and SiWA−H_3PO_4−PVA-based cells at high frequencies. (c) The water retention effect influences the environmental stability of the electrolyte as well as the dynamic dissociation of water molecules in the SiWA structure, impacting both proton density and proton mobility. Both SiO_2 and TiO_2 fillers improved environmental stability of the electrolyte, and SiWA−H_3PO_4−PVA/SiO_2 demonstrated a higher water retention effect and the least fluctuation of proton conductivity with relative humidity. A stronger water retention effect of SiO_2 at higher temperatures ensured a more stable proton transport network in the electrolyte and maintained high proton mobility.

While the functions of SiO_2 and TiO_2 nanofillers in solid SiWA−H_3PO_4−PVA are complex, dielectric analysis provides a powerful method to differentiate these functions at different operating conditions. Using a single-ion approach, the temperature dependent proton conduction properties can be derived. These data could be used to answer key questions regarding the design of highly conductive polymer electrolytes. For example, it is clearly indicated that an optimization of proton density and proton mobility, particularly in the HPA-based electrolyte system, is critical to reach maximum proton conductivity and desirable supercapacitor performance.

dx.doi.org/10.1021/am4045103 | ACS Appl. Mater. Interfaces 2014, 6, 464−472

AUTHOR INFORMATION

Corresponding Author

*E-mail: keryn.lian@utoronto.ca.

Author Contributions

The manuscript was written through contributions of all authors. All authors have given approval to the final version of the manuscript.

Notes

The authors declare no competing financial interest.

ACKNOWLEDGMENTS

We appreciate the financial support from NSERC Canada. H. Gao would like to acknowledge an NSERC Alexander Graham Bell Canada Graduate Scholarship.

REFERENCES

(1) Hardwick, A.; Dickens, P. G.; Slade, R. C. T. *Solid State Ionics* **1984**, *13*, 345−350.
(2) Kreuer, K. D.; Hampele, M.; Dolde, K.; Rabenau, A. *Solid State Ionics* **1988**, *28*−*30* (Part 1), 589−593.
(3) Slade, R. C. T.; Pressman, H. A.; Skou, E. *Solid State Ionics* **1990**, *38*, 207−211.
(4) Slade, R. C. T.; Barker, J.; Pressman, H. A. *Solid State Ionics* **1988**, *28*−*30* (Part 1), 594−600.
(5) Mioč, U. B.; Todorović, M. R.; Davidović, M.; Colomban, P.; Holclajtner-Antunović, I. *Solid State Ionics* **2005**, *176*, 3005−3017.
(6) Micek-Ilnicka, A. *J. Mol. Catal. A: Chem.* **2009**, *308*, 1−14.
(7) Nakamura, O.; Ogino, I.; Kodama, T. *Solid State Ionics* **1981**, *3*−*4*, 347−351.
(8) Mioč, U.; Colomban, P.; Novak, A. *J. Mol. Struct.* **1990**, *218*, 123−128.
(9) Kremenović, A.; Spasojević-de Biré, A.; Dimitrijević, R.; Sciau, P.; Mioč, U. B.; Colomban, P. *Solid State Ionics* **2000**, *132*, 39−53.
(10) Staiti, P.; Freni, S.; Hocevar, S. *J. Power Sources* **1999**, *79*, 250−255.
(11) Herring, A. M. *J. Macromol. Sci., Polym. Rev.* **2006**, *46*, 245−296.
(12) Lavrenčič Štangar, U.; Grošelj, N.; Orel, B.; Colomban, P. *Chem. Mater.* **2000**, *12*, 3745−3753.
(13) Gao, H.; Lian, K. *J. Electrochem. Soc.* **2011**, *158*, A1371−A1378.
(14) Gao, H.; Lian, K. *J. Power Sources* **2011**, *196*, 8855−8857.
(15) Gao, H.; Lian, K. *J. Electrochem. Soc.* **2013**, *160*, A505−A510.
(16) Young, G. J. *J. Colloid Sci.* **1958**, *13*, 67−85.
(17) Finnie, K. S.; Cassidy, D. J.; Bartlett, J. R.; Woolfrey, J. L. *Langmuir* **2001**, *17*, 816−820.
(18) Shanmugam, S.; Viswanathan, B.; Varadarajan, T. K. *J. Membr. Sci.* **2006**, *275*, 105−109.
(19) Jin, Y.; Qiao, S.; Zhang, L.; Xu, Z. P.; Smart, S.; Costa, J. C. D. d.; Lu, G. Q. *J. Power Sources* **2008**, *185*, 664−669.
(20) Shao, Z.-G.; Joghee, P.; Hsing, I. M. *J. Membr. Sci.* **2004**, *229*, 43−51.
(21) Pereira, F.; Vallé, K.; Belleville, P.; Morin, A.; Lambert, S.; Sanchez, C. *Chem. Mater.* **2008**, *20*, 1710−1718.
(22) Zaborski, M.; Vidal, A.; Ligner, G.; Balard, H.; Papirer, E.; Burneau, A. *Langmuir* **1989**, *5*, 447−451.
(23) Klein, R. J.; Zhang, S.; Dou, S.; Jones, B. H.; Colby, R. H.; Runt, J. *J. Chem. Phys.* **2006**, *124*, 144903.
(24) Macdonald, J. R. *Phys. Rev.* **1953**, *92*, 4−17.
(25) Macdonald, J. R. *J. Chem. Phys.* **1974**, *61*, 3977−3996.
(26) Coelho, R. *J. Non-Cryst. Solids* **1991**, *131*−*133* (Part 2), 1136−1139.
(27) Tjapkin, N.; Davidović, M.; Colomban, P.; Mioč, U. *Solid State Ionics* **1993**, *61*, 179−185.
(28) Fragiadakis, D.; Dou, S.; Colby, R. H.; Runt, J. *Macromolecules* **2008**, *41*, 5723−5728.
(29) Fragiadakis, D.; Dou, S.; Colby, R. H.; Runt, J. *J. Chem. Phys.* **2009**, *130*, 064907−11.
(30) Li, Y.; Huang, X.; Hu, Z.; Jiang, P.; Li, S.; Tanaka, T. *ACS Appl. Mater. Interfaces* **2011**, *3*, 4396−4403.
(31) Zhou, T.; Zha, J.-W.; Cui, R.-Y.; Fan, B.-H.; Yuan, J.-K.; Dang, Z.-M. *ACS Appl. Mater. Interfaces* **2011**, *3*, 2184−2188.
(32) Popielarz, R.; Chiang, C. K.; Nozaki, R.; Obrzut, J. *Macromolecules* **2001**, *34*, 5910−5915.
(33) Smith, T. W.; Abkowitz, M. A.; Conway, G. C.; Luca, D. J.; Serpico, J. M.; Wnek, G. E. *Macromolecules* **1996**, *29*, 5042−5045.
(34) Choi, U. H.; Lee, M.; Wang, S.; Liu, W.; Winey, K. I.; Gibson, H. W.; Colby, R. H. *Macromolecules* **2012**, *45*, 3974−3985.
(35) Wang, D.; Bao, Y.; Zha, J.-W.; Zhao, J.; Dang, Z.-M.; Hu, G.-H. *ACS Appl. Mater. Interfaces* **2012**, *4*, 6273−6279.
(36) Robertson, J. *Eur. Phys. J. Appl. Phys.* **2004**, *28*, 265−291.
(37) Taberna, P. L.; Simon, P.; Fauvarque, J. F. *J. Electrochem. Soc.* **2003**, *150*, A292−A300.
(38) Sirdeshmukh, D. B.; Sirdeshmukh, L.; Subhadra, K. G. *Micro- and Macro-Properties of Solids*; Springer: Berlin Heidelberg, 2006; Vol. *80*, pp 199−255.